Journal of Power Sources 270 (2014) 403–410

Contents lists available at ScienceDirect

Journal of Power Sources

journal homepage: www.elsevier.com/locate/jpowsour

# Simple synthesis of hierarchical porous carbon from *Enteromorpha prolifera* by a self-template method for supercapacitor electrodes

Yuan Gao [a], Wenli Zhang [b], Qinyan Yue [a, *], Baoyu Gao [a], Yuanyuan Sun [a], Jiaojiao Kong [a], Pin Zhao [a]

[a] Shandong Provincial Key Laboratory of Water Pollution Control and Resource Reuse, School of Environmental Science and Engineering, Shandong University, Jinan 250100, China
[b] College of Chemistry, Jilin University, Changchun 130012, China

## HIGHLIGHTS

- A simple self-template method was used to fabricate hierarchical porous carbons.
- *Enteromorpha prolifera*, a green algae, served as carbon precursor.
- The hierarchical porous carbon presented a high surface area of 3332 $m^2 g^{-1}$.
- The hierarchical porous carbons showed excellent capacitive behavior.

## GRAPHICAL ABSTRACT

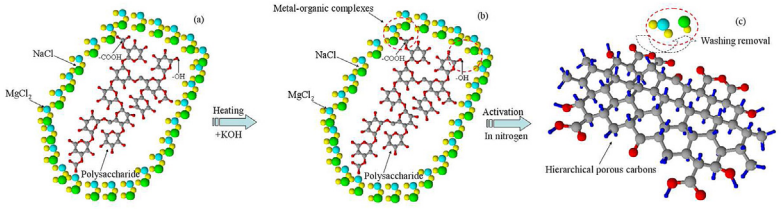


## ARTICLE INFO

*Article history:*
Received 19 February 2014
Received in revised form
28 May 2014
Accepted 18 July 2014
Available online 24 July 2014

*Keywords:*
Hierarchical porous carbon
Self-template method
High surface area
Electrochemical properties

## ABSTRACT

Hierarchical porous carbons (HPCs) with high specific surface area are synthesized by a simple self-template strategy from the alage *Enteromorpha prolifera* (*E. prolifera*). The surface of the dried *E. prolifera* biomass contains carboxylic/hydroxyl groups and mineral salts, which can cooperate together to form metal-organic framework complexes. These salts and complexes can serve as self-templates to produce hierarchical porous structures during the activation process. The activated carbon is used to make an HPC electrode and the electrochemical properties of the supercapacitor fabricated from this HPC electrode are characterized by cyclic voltammetry, galvanostatic charge–discharge and electrochemical impedance spectroscopy in 6 mol $L^{-1}$ KOH solution. The specific capacitance is 210 F $g^{-1}$ at a current density of 3 A $g^{-1}$. The good capacitive behavior is attributed to the high BET-surface area of 3332 $m^2 g^{-1}$, large pore volume of 2.46 $cm^3 g^{-1}$ and hierarchical porous structure (an abundance of interconnected mesopores, macropores and micropores). These results demonstrate that *E. prolifera* is a promising precursor to prepare high performance and low cost electrode materials for electrical double layer capacitors (EDLCs).



## 1. Introduction

Supercapacitor (or electrochemical capacitor) is one of the most important energy storage devices, because they excel at providing high energy within a short period of time and supplying back-up power to avoid power losses [1–3]. According to different charge storage mechanisms, supercapacitors can be generally classified into two types: pseudocapacitors and electrical double layer capacitors (EDLCs). Compared to pseudocapacitors or conventional batteries, EDLCs exhibit a long cycle life (>$10^6$ circles), excellent rate capability and superior power density (10 kW $kg^{-1}$) [4]. Currently, EDLC electrode materials, e.g., porous carbons, conducting

* Corresponding author. Tel.: +86 531 88365258; fax: +86 531 88364513.
*E-mail address:* qyyue58@aliyun.com (Q. Yue).

http://dx.doi.org/10.1016/j.jpowsour.2014.07.115
0378-7753/

polymers and transition-metal oxides, are widely investigated. Among them, porous carbon materials are considered to be the most promising candidates for EDLC electrodes due to their large specific surface area, excellent chemical stability and relatively low cost [5].

Activated carbon (AC) is the most commonly used porous carbon material for EDLC electrodes [6–9]. The pore structure and the specific surface area of ACs have significant influence on the ion storage capacity and diffusion rate of the supercapacitor. Micropores can significantly enhance the surface area of a porous carbon material and increase the capacitance of the electrode. However, tortuous micropores in ACs could hinder the diffusion for electrolyte ions into the pores, resulting in poor rate capability at high current density. In contrast, the presence of excess mesopores and macropores in ACs could lead to smaller surface area, while reducing the capacitance and energy density. Hence, efforts to develop high performance electrode materials with good electrochemical properties are of great importance. Hierarchical porous carbons with a rational combination of micropores, mesopores and macropores are considered as promising supercapacitor electrode materials [10–12]. Up to now, soft/hard template techniques have been widely employed to synthesize HPCs. The templates commonly involve $SiO_2$, ZnO, zeolite, surfactant or polystyrene [13–17]. Górka et al. reported the use of tetraethyl orthosilicate-generated silica and colloidal silica as hard template and ethylene oxide-propylene oxide-ethylene oxide triblock copolymer as soft template for preparation of HPCs [18]. Pérez-Cabero et al. synthesized HPCs employing alumino-silica UVM-7 as hard template [19]. These processes are complicated and time-consuming due to the multiple activation processes and the requirements for additional steps to remove the special templates. Self-template or template-free methods have also been used for HPC synthesis with banana peel, starch or animal bone as precursors [10–12]. However, additional carbon sources, stabilization pretreatment or strict operation conditions were required in these synthetic processes. Thus, these synthesis methods for HPCs are uncompetitive in terms of their price-to-performance ratio which restricts their application to mass-production.

Herein, we report a simple and cost-effective self-template strategy for the fabrication of HPCs from *Enteromorpha prolifera* (*E. prolifera*). *E. prolifera* is a green algae, which consists of biopolymers, protein and a certain amount of mineral salts (e.g., sodium chloride) [20]. The underlying hypothesis of this study is that the organic materials of *E. prolifera*, as well as the salts and metal-organic complexes can serve as carbon precursors and natural, soluble, structure-directing templates for the formation of meso/micro pores. *E. prolifera* has channel-like walls and a plywood-like lamellae sub-microstructure which could be helpful for the formation of a hierarchical porous structure in the carbon materials. Additionally, *E. prolifera*, a natural marine waste, is inexpensive, environmentally benign and abundantly available [21]. Synthesis of high-quality HPCs from this low-value carbon source develops an effective way to turn this biomass waste into a high-value-added product. The results indicate that the prepared HPCs display high specific capacitance and are a promising electrode material for supercapacitors.

## 2. Experimental

### 2.1. Materials and chemicals

*E. prolifera* was collected from the seashore of the Yellow Sea (Qingdao, China). *E. prolifera* was dried in sunlight, ground and sieved to 0.425 mm before the preparation process. Potassium hydroxide was purchased from Sinopharm (Beijing, China) and used without further purification. Ethanol was of analytical grade from Sinopharm (Beijing, China) and used as received. Hydrochloric acid was commercially available from Fu Yu Corp. (Tianjin, China). Polytetrafluorethylene (PTFE; 60%) and acetylene black (electronic grade) were provided by Li Yuan Corp. (Taiyuan, China).

### 2.2. Preparation of HPCs

The formation process of the HPCs was based on a simple and reproducible strategy. Firstly, *E. prolifera* was carbonized at a heating rate of 15 °C $min^{-1}$ up to 500 °C. The carbonization was maintained at this desired temperature for 1.5 h by using our laboratory's self-designed chamber-type electric resistance furnace (KSY-4D-16). Then the resultant char was mixed with potassium hydroxide powder (about 0.15 mm) through grinding using a ceramic mortar for 30 min. Afterwards, the samples were subjected to activation under nitrogen at 750 °C for 1 h. After cooling to room temperature, the obtained samples were washed with hot water, hydrochloric acid (1N) and distilled water to remove residual potassium hydroxide. Different mass ratios of KOH/char in the range of 1–3 were investigated. The samples synthesized this way were called grind derived-activated carbon, namely GAC. The various carbon materials prepared by changing the proportion of KOH to char were marked as GAC-1, GAC-2 and GAC-3.

For comparison, the carbons were also prepared by a solution mixing method. The synthesis was performed as described previously except that the carbonized char was first soaked in aqueous potassium hydroxide solution (50%) for 12 h at the same weight ratios as above. Then the mixture was dried at 110 °C for 48 h to guarantee the water was totally evaporated. The carbons prepared by this method were named solution derived-activated carbon, or

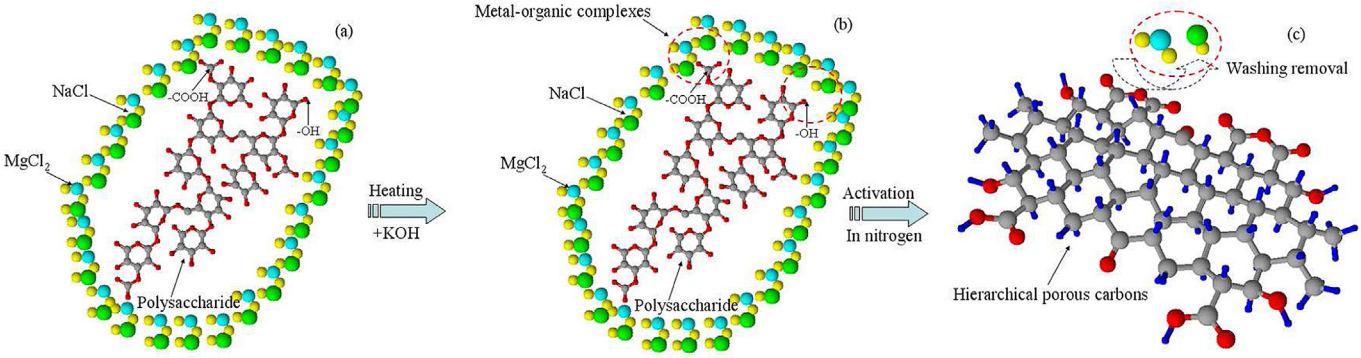


**Fig. 1.** Schematic representation of the formation process of hierarchical porous carbons frameworks.

SAC. The carbon materials prepared by changing the proportion of KOH to char were marked as SAC-1, SAC-2 and SAC-3. The detailed synthesis is given in Scheme 1 in the Supporting information. All preparation experiments were carried out in triplicate and the average values were reported.

Fig. 1 shows the proposed mechanism of formation of the HPCs. As can be seen in Fig. 1a, the main ingredients of *E. prolifera* are polysaccharides [22], which were used as carbon resource. Also, there are many functional groups and a number of mineral salts, such as sodium chloride and magnesium chloride, on the surface of *E. prolifera* [23]. The salts cooperated with the hydroxyl groups or carboxylic groups to co-assemble into metal-organic complexes (Fig. 1b), thus acting as a self-template for the formation of hierarchical porous carbon [11]. In addition, the salts themselves also served as an *in situ* structure-directing template for the formation of micropores/mesopores. The potassium hydroxide and its corresponding species were employed as graphitization catalysts. After activation, the salts were removed easily by a conventional washing process (Fig. 1c).

### 2.3. Characterization

The porous textures of the prepared carbons were characterized by $N_2$ adsorption and desorption experiments at 77 K (JW-BK122W, Beijing JWGB Sci. & Tech. Co., China). Prior to analysis, the samples were degassed in vacuum at 473 K for at least 2 h. The specific surface area was calculated according to the Brunauer–Emmet–-Teller (BET) method. The total pore volume was calculated from the adsorption amount of $N_2$ at a relative pressure of 0.99. The pore size distribution was obtained from the adsorption branch of the isotherms by using the Barrett–Joyner–Halenda (BJH) method. The morphologies of the samples were studied using SEM (JEOL, JSM 7600F, Japan). The crystallinities of the samples were analyzed using a Rigaku D/MAX-YA diffractometer with Cu-Ka radiation as X-ray source. The surface chemical characterizations of the samples were performed using Fourier transform infrared (FTIR) spectroscopy (Avatar 370).

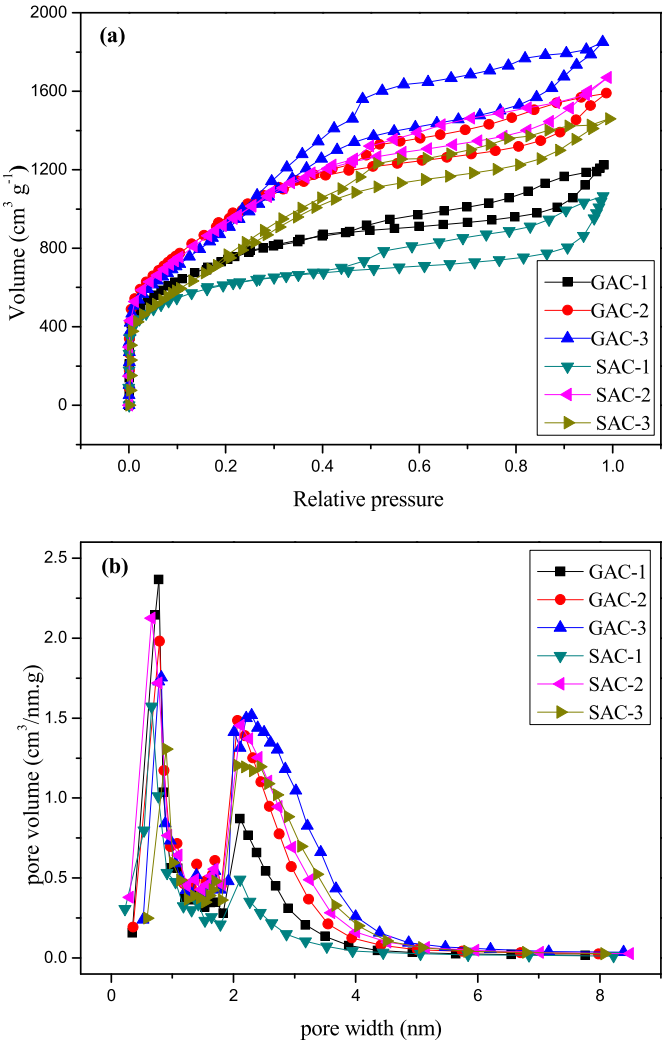


**Fig. 2.** (a) Nitrogen adsorption–desorption isotherms and (b) pore size distributions of the prepared hierarchical porous carbons.

### 2.4. Electrochemical measurements

The test electrode was fabricated by mixing 85 wt.% carbon sample as active material, 10 wt.% acetylene black as conductive material and 5% polytetrafluorethylene as binder. The blend was kneaded thoroughly using an agate mortar in ethanol solution. Then the blend was pressed into a square sheet with a surface area of 100 mm$^2$ (10 × 10 mm) at 10 MPa. The sheet was dried at 100 °C overnight. The dried sheet was pressed onto a nickel foam collector. The loading of active material on the dried electrodes was in the range of 2–5 mg cm$^{-2}$. Two identical electrodes were assembled into a supercapacitor, isolated with two layers of porous separator membranes.

Cyclic voltammetry (CV), galvanostatic charge–discharge (GCD) and electrochemical impedance spectroscopy (EIS) experiments were performed using a PARSTAT2273 electrochemical workstation at room temperature with 6 M KOH as electrolyte. The CV tests were recorded within a potential window of 0–1.0 V at various scan rates ranging from 10 to 100 mV s$^{-1}$. The GCD experiments were carried out from 0 to 1.0 V with different current densities from 0.125 to 3 A g$^{-1}$. The EIS measurements were carried out with the potential amplitude of 10 mV over the frequency range from 100 kHz to 100 mHz. The specific capacitances are calculated as follows [1]:

$$C_{GCD} = \frac{I\Delta t}{m\Delta V} \times 2 \quad (1)$$

$$C_{CV} = \frac{\int Idu}{2\nu(2m)\Delta V} \times 4 \quad (2)$$

where $C_{GCD}$ and $C_{CV}$ are the specific capacitances calculated from the GCD test and CV test, respectively (F g$^{-1}$). $I$ is the current load (A), $\Delta t$ is the discharge time (s), $m$ is the mass of active material (g), $\Delta V$ is potential range (V) and $\nu$ is scan rate (mV s$^{-1}$).

The electrochemical impedance $Z(\omega)$ is calculated according to the following equation [24]:

$$Z(\omega) = Z'(\omega) + jZ''(\omega) \quad (3)$$

where $Z'(\omega)$ and $Z''(\omega)$ are the real and imaginary parts of the impedance $Z(\omega)$, respectively; $\omega$ is the angular frequency, which is obtained based on $\omega = 2\pi f$. The capacitance of the supercapacitor $C(\omega)$ is composed of two parts: the real part $C'(\omega)$, corresponding to the static capacitance of the cell; and the imaginary part $C''(\omega)$, relevant to energy dissipation by an irreversible faradaic charge transfer process [25]. $C(\omega)$ is defined based on the complex capacitance model reported by Taberna et al. [26].

**Table 1**
Textural properties of the prepared hierarchical porous carbons.

| Sample | $S_{BET}$ ($m^2\ g^{-1}$) | $V_{tol}$ ($cm^3\ g^{-1}$) | $V_{micro}$ ($cm^3\ g^{-1}$) | $V_{meso}$ ($cm^3\ g^{-1}$) | $V_{micro}/V_{tol}$ (%) | $D_{AC}$ (nm) |
|---|---|---|---|---|---|---|
| GAC-1 | 2640.1 | 1.893 | 0.854 | 1.039 | 46.11 | 2.869 |
| GAC-2 | 3332.3 | 2.460 | 0.975 | 1.485 | 39.63 | 2.953 |
| GAC-3 | 3140.6 | 2.863 | 0.273 | 2.590 | 9.54 | 3.647 |
| SAC-1 | 2200.8 | 1.649 | 0.803 | 0.846 | 48.70 | 2.998 |
| SAC-2 | 3302.5 | 2.584 | 0.785 | 1.799 | 31.38 | 3.130 |
| SAC-3 | 2622.4 | 2.257 | 0.357 | 1.900 | 15.82 | 3.443 |

$S_{BET}$: BET specific surface area.
$V_{tol}$: Total pore volume.
$V_{micro}$: Micropore volume.
$V_{meso}$: Mesopore volume.
$D_{AC}$: Average pore size.

$$C'(\omega) = \frac{-Z''(\omega)}{\omega|Z(\omega)|^2} \tag{4}$$

$$C''(\omega) = \frac{Z'(\omega)}{\omega|Z(\omega)|^2} \tag{5}$$

The maximum energy $E$ (Wh $kg^{-1}$) is calculated at a scan rate of 10 mV $s^{-1}$ based on the following equation:

$$E = \frac{1}{2} C_{CV} \Delta V^2 \tag{6}$$

## 3. Results and discussion

### 3.1. Surface area and pore structure

The $N_2$ adsorption–desorption isotherms are shown in Fig. 2. The isotherms of all samples were a typical mixture of type I and type IV, indicating the coexistence of mesopores and micropores. According to IUPAC, the pores of a carbon material can be divided into three types: micropores (<2 nm), mesopores (2–50 nm) and macropores (>50 nm). The steep increase in $N_2$ uptake volume at low relative pressure was related to the micropores filling [27]. The remarkable hysteresis loop, occurring at relative pressures in the range of 0.45–0.9, was attributed to the capillary condensation in mesopores [28,29]. Moreover, another $N_2$ uptake was observed at high relative pressure of 0.95–1.0 due to the macropores. Fig. 2b reveals that most pores were in the region of ultrafine micropores (<1 nm) and narrow mesopores (2–4 nm). With the increase of KOH/char ratio, the peak maxima related to the mesopores were shifted towards larger pores and the peaks became wider. The porous texture parameters are summarized in Table 1. All samples displayed impressively high surface area, varying from 2640 to 3332 $m^2\ g^{-1}$ and 2200–3302 $m^2\ g^{-1}$ for GAC and SAC, respectively. With the increasing ratio of KOH, the surface area increased to a maximum and then declined, while the percentage of micropore decreased steadily from 46.11% to 9.54% and 48.70%–15.82% for GAC and SAC, respectively. As the dosage of KOH increased, the carbon layer continued to react with the excess KOH and the existing micropores gradually transformed into new mesopores or macropores. Concurrently, the average pore size increased from 2.869 to 3.647 nm and 2.998–3.443 nm for GAC and SAC, respectively. The average pore size of all samples was ~3 nm, which may facilitate the accessibility of electrolyte ions into the internal pores during the electrochemical processes [30].

### 3.2. Morphology analysis

SEM technology was employed to investigate the surface morphologies of the carbons. The morphology of *E. prolifera* is displayed in Fig. S1. Large quantities of fine salt particles can be observed on the surface of *E. prolifera*. Furthermore, according to our previous study [23], there were also many carboxylic and hydroxyl groups in *E. prolifera*, which can coordinate with salt ions to form metal-organic complexes during the activation process. The complexes served as self-templates or space fillers to produce the hierarchical porous structure. The XRD patterns exhibit no residual salts in the HPCs (see Fig. S2), which confirmed that the salts could be removed easily by conventional washing, thus no additional template removal process was required. The SEM images in Fig. 3

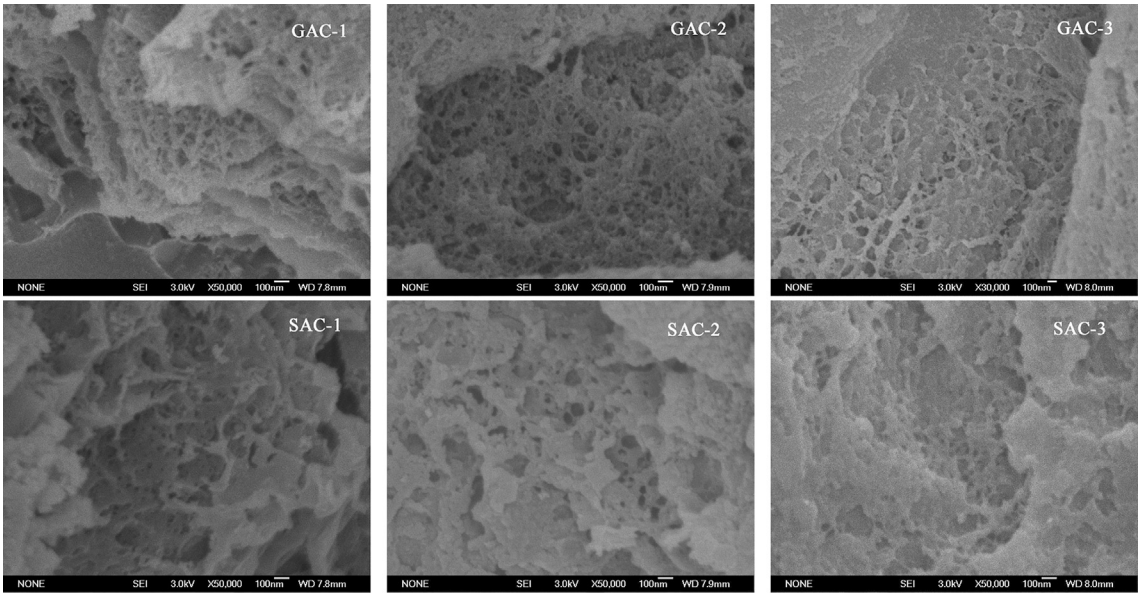


**Fig. 3.** SEM images of the prepared hierarchical porous carbons.

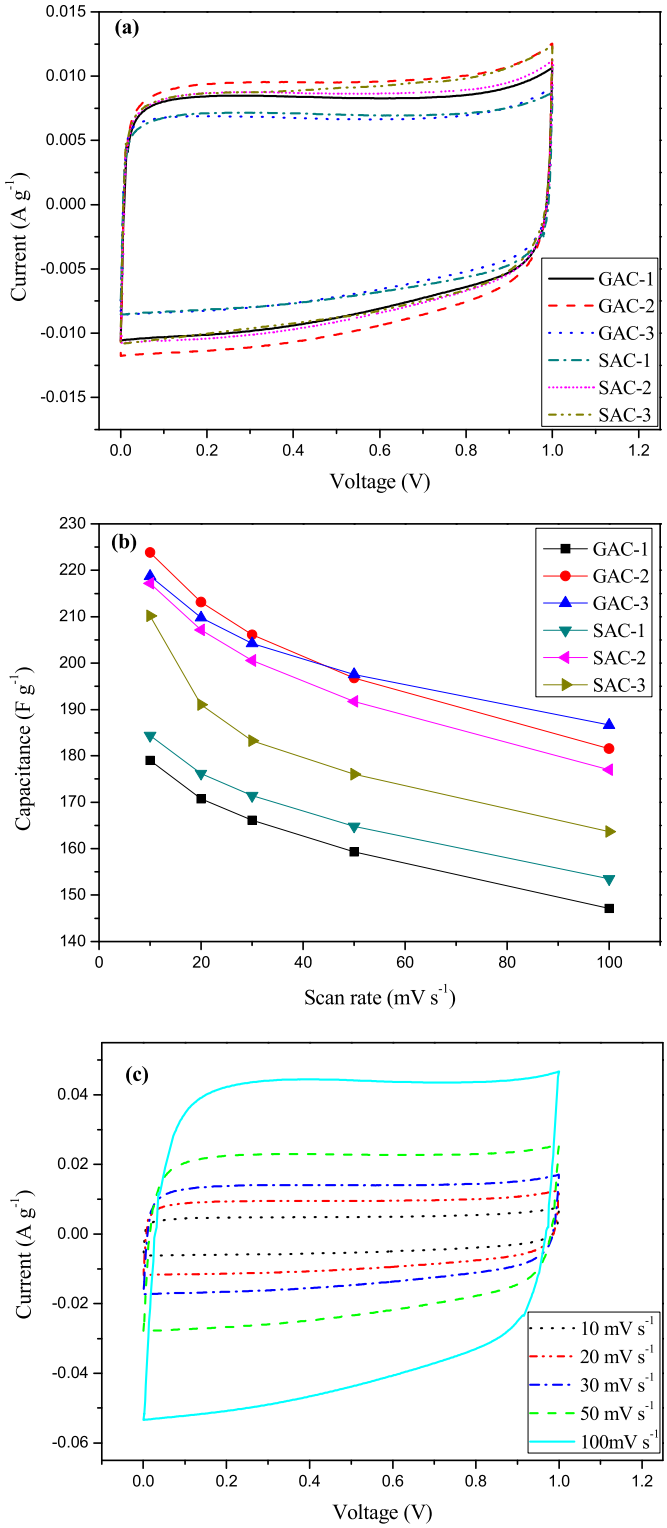


**Fig. 4.** (a) Cyclic voltammetry curves of the prepared carbons taken at a scan rate of 20 mV s$^{-1}$, (b) variation of $C_{CV}$ with scan rate in the carbons and (c) cyclic voltammetry curves of GAC-2 at different scan rates.

demonstrate the presence of not only micropores, but also mesopores and macropores. The mesopores and macropores have diameters ranging from 10 to 100 nm. Compared to the SACs, the pores on the GACs were relatively non-uniform in size and highly disperse in shape, which facilitated the formation of an irregular honeycomb-like nanostructure. Thus the hierarchical pore structure may endow the carbon with outstanding capacitive performance.

### 3.3. Surface functional groups

FT-IR test was performed to observe the surface chemical properties of the carbons, which may trigger electrochemical activity in the electrolyte solution during the electrochemical tests. The FT-IR spectra (see Fig. S3) display noticeable peaks around 3400 and 1100 cm$^{-1}$. The former is ascribed to N–H or O–H stretching vibrations [31,32], while the latter may belong to C–O or C–O–C stretching modes. The peaks around 1100 cm$^{-1}$ gradually disappeared with the increase of KOH/char ratio, which was due to further decomposition and dehydration reactions. More importantly, there were no conspicuous humps on the cyclic voltammetry or charge–discharge curves, implying that no oxidation–reduction reaction was induced by the heteroatoms. In other words, scarcely any pseudocapacitance contributed to the capacitance of the carbon electrodes.

### 3.4. Electrochemical performance

#### 3.4.1. Cyclic voltammetry tests

Cyclic voltammetry was performed to estimate the capacitance of the electrodes at a series of scan rates. Fig. 4a shows the CV curves of different carbons at a scan rate of 20 mV s$^{-1}$. The CV curves present rectangular-like shapes without any redox peaks, indicating the absence of strong pseudocapacitive phenomena and the existence of an ideal double-layer capacitive characteristic of the carbon electrode. The values of capacitance at various scan rates are presented in Table 2. The values of capacitance decrease in the order of GAC-2 > GAC-3 > SAC-2 > SAC-3 > SAC-1 > GAC-1. However, the BET surface area of the carbons did not follow the same sequence, which indicated that the capacitance was not only related to specific surface area but also associated with other characteristic, such as pore size distribution or functional groups. In addition, GACs displayed slightly higher capacitance than the SACs. The highest $C_{CV}$ for GAC-1, GAC-2 and GAC-3 were 210.6 F g$^{-1}$, 263.4 F g$^{-1}$ and 257.3 F g$^{-1}$, respectively. As shown in Fig. 4b, the capacitance $C_{CV}$ reduced with the increased scan rates, because the electrical double layer in the micropores could not respond as quickly as the rate of change in electrical potential. However, the hierarchical pores still contributed to a smooth and easy movement of the electrolyte ions, even at a high scan rate of 100 mV s$^{-1}$. The CV plots of a GAC-2 electrode at different scan rates are shown in Fig. 4c. The CV curves exhibited a typical "box-like" shape and no obvious polarization at high scan rates, indicating quick dynamics of charge transmission for the electrodes and small resistance in approachable pores [1]. The synergistic effects of large surface area and hierarchical porous structure facilitated an excellent capacitance of ~250 F g$^{-1}$ and good capacitance retention of ~80%.

#### 3.4.2. Electrochemical impedance spectroscopy tests

Electrochemical impedance spectroscopy measurements were carried out to obtain the complementary performance information related to the frequency response and further understand the electrochemical behavior of the HPC electrodes [33]. Table 3 shows the parameters derived from the fitting data of the Nyquist plots using the ZSimpWin software according to the equivalent circuit (Fig. S4). Fig. 5a illustrates the Nyquist plots for the devices with HPC electrodes. The impedance behavior varies from a pure capacitance at low frequency to a pure resistance at high frequency

**Table 2**
The specific gravimetric capacitance of the prepared hierarchical porous carbons at different scan rates.

| Sample | $C_{CV}$ at different voltage scan rates (F $g^{-1}$) | | | | | |
|---|---|---|---|---|---|---|
| | 10 mV $s^{-1}$ | 20 mV $s^{-1}$ | 30 mV $s^{-1}$ | 50 mV $s^{-1}$ | 100 mV $s^{-1}$ | Retention% |
| GAC-1 | 210.6 | 200.8 | 195.4 | 187.4 | 173.1 | 82.18 |
| GAC-2 | 263.4 | 250.7 | 242.5 | 231.4 | 213.5 | 81.06 |
| GAC-3 | 257.3 | 246.8 | 240.3 | 232.4 | 219.6 | 85.36 |
| SAC-1 | 216.9 | 207.3 | 201.6 | 193.9 | 180.6 | 83.24 |
| SAC-2 | 255.5 | 244.2 | 235.9 | 225.5 | 208.2 | 81.49 |
| SAC-3 | 247.3 | 224.8 | 215.5 | 207.1 | 192.6 | 77.87 |

for all supercapacitors. At low frequencies, the curves were almost vertical, implying a near-ideal electric double layer capacitive nature. In the region of medium frequencies Warburg impedance was observed, where the electrolyte ion penetrated into the depth of the micro/mesoporous network of the electrode materials [25,34]. At high frequencies, the capacitor behavior in EIS was illustrated by the semi-circle plots. This behavior was related to the porous structures and functional groups of the electrode material [25]. At high frequencies, the capacitance was poorly developed, because the abundant charge transfer complexes have difficulty overcoming the activation energy to move with the rapid variation of the potential [35]. The low values of charge transfer resistance $R_{ct}$ (<0.1 Ω) indicated better electrolyte accessibility into the micropores of the electrode materials [35].

The first intersection point of the Nyquist plots on the real axis reflects the value of equivalent series resistance (ESR). The ESR consists of three parts: the ionic resistance of the KOH electrolyte, the inherent resistance of the electrode material and the contact resistance at the interface between the current collector and the active material. Obviously, all the electrodes have relatively low ESR, which may stem from the reasonable surface wetting ability as a result of the polar groups on the surface of HPCs (see Fig. S3). The results in Table 3 demonstrate that the values of ESR were lower for the GACs than the SACs, indicating better electrode conductivity in the former case. As the electrolyte was same for all devices, the ionic resistance of the KOH electrolyte should be constant. The difference in ESR may be mainly attributed to the different resistances of various carbon electrode materials. The SEM micrographs (Fig. 3) indicate that there are more irregular and disordered pore structures in the GACs.

The impedance behavior was further analyzed by applying the model of complex capacitance, which assumes that the supercapacitor behaves like a series combination of a capacitor and a resistor, and its behavior depends rely on the frequency. The plots of normalized $C'(\omega)$ and $C''(\omega)$ vs frequency are presented in Fig. 5b and c. Fig. 5b shows that the plots of $C'(\omega)$ vs frequency could be distinguished into three parts. At low frequencies, the capacitance sharply increased with the decrease of the frequency and reached maximum. During this stage, the electrolyte ions could diffuse into almost all the pores. At very high frequencies, the behavior of this system corresponded to a pure resistor. The value of capacitance tended to zero, because the electrolyte ions could only reach the outer space without entering into the depth of the pores. Also, a transition region was observed between these two frequencies, where the capacitance decreased linearly with the increase of the frequency. This result is consistent with other reports [26,36]. Fig. 5c shows the imaginary part of the capacitance reaches a maximum at frequency $f_0$, which was used to define a time constant. The relaxation time $t_0$ is calculated according to $t_0 = 1/f_0$. The relaxation time is the time required to transfer the power and energy efficiently, which is the boundary between the resistive and capacitive behavior of the device. The relaxation time was ~1 s for all samples, thus allowing a fast energy delivery in the supercapacitors. This behavior was attributed to a small equivalent series resistance due to the excellent multi-level pore network of the electrode material. Moreover, the maximum energies were 24.86 Wh $kg^{-1}$ and 29.19 Wh $kg^{-1}$ for GAC-1 and SAC-3 electrodes, respectively. As the specific surface areas of both carbons were similar, the difference in maximum energy may mainly derive from the enhanced ions transfer efficiency of the abundant mesopores in SAC-3.

### 3.4.3. *Galvanostatic charge–discharge tests*

Galvanostatic charge–discharge measurements were conducted to evaluate the relationship between the capacitance and the current density. According to the CV and EIS results, GAC-2 displayed the best electrochemical performance. Therefore, GAC-2 was regarded as a typical sample to investigate charge–discharge cycling at various current densities. The charge–discharge curves present a virtually linear shape at different loading current densities from 0.5 to 3 A $g^{-1}$, implying no obvious distortions due to pseudocapacitance and excellent capacitor behavior for the HPC electrodes. Fig. 6a shows that a small IR drop occurred at the beginning of the discharge stage, indicating weak energy dissipation due to internal resistance of the HPC electrodes. As shown in Fig. 6b, the capacitance of HPCs declined slightly with the increasing current densities from 0.125 to 3 A $g^{-1}$. The specific capacitance of HPCs was 275 F $g^{-1}$ at a current density of 0.125 A $g^{-1}$, while the specific capacitance was still 210 F $g^{-1}$ at a high current density of 3 A $g^{-1}$ with a good retention of 76%. The excellent performance could make this promising electrode material fulfill the requirements of high performance supercapacitors, especially high power density and rate capability.

## 4. Conclusions

High performance electrode materials for supercapacitors were synthesized from *E. prolifera* by a simple self-template strategy. The specific capacitance of HPCs electrode was 275 F $g^{-1}$ at a current density of 0.125 A $g^{-1}$ and still displayed relative high of 210 F $g^{-1}$

**Table 3**
Electrochemical parameters for EDLCs.

| Sample | GAC-1 | GAC-2 | GAC-3 | SAC-1 | SAC-2 | SAC-3 |
|---|---|---|---|---|---|---|
| ESR (Ω) | 0.1367 | 0.1310 | 0.1324 | 0.1593 | 0.1554 | 0.1622 |
| $R_{ct}$ (Ω) | 0.0175 | 0.0182 | 1.01E-6 | 0.0394 | 1.04E-7 | 1.03E-7 |
| $E_{max}$ (Wh $kg^{-1}$) | 24.86 | 31.09 | 30.38 | 25.61 | 30.16 | 29.19 |

ESR: Equivalent series resistance.
$R_{ct}$: Charge transfer resistance.
$E_{max}$: Maximum energy.

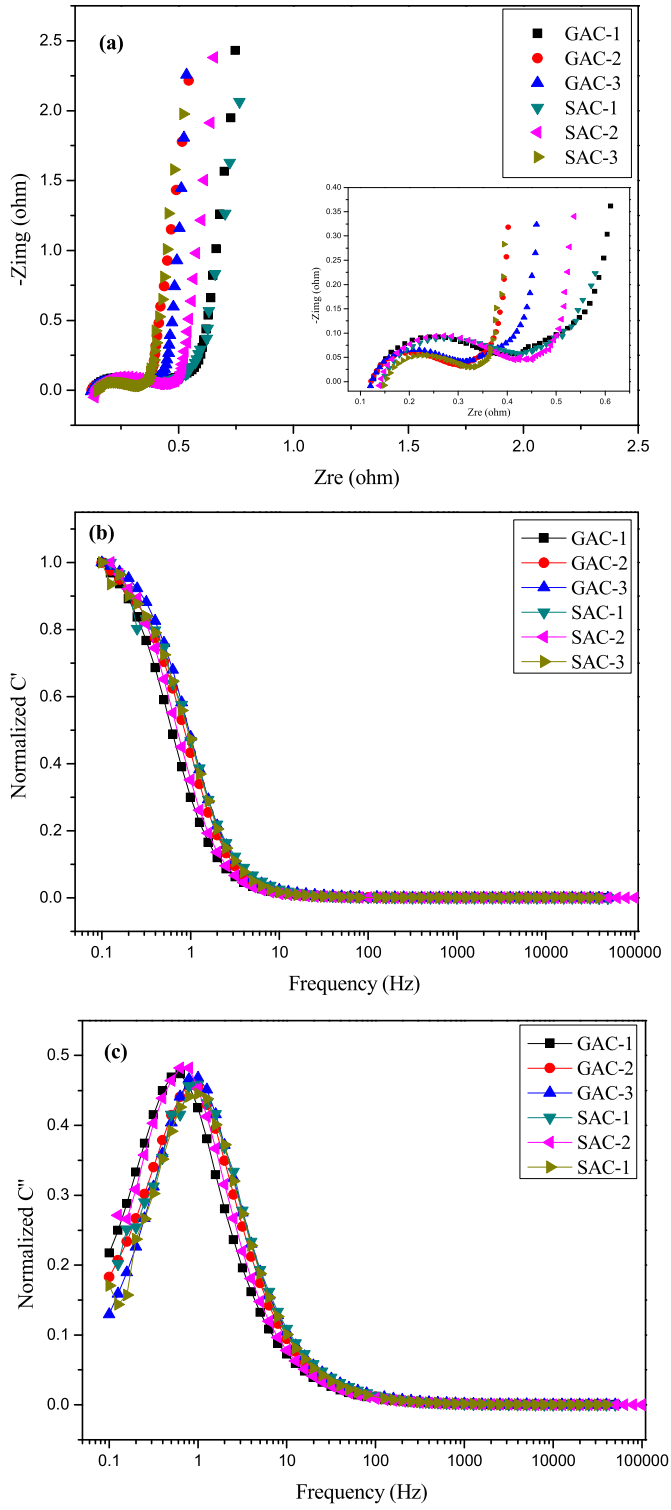


**Fig. 5.** (a) Nyquist plot of the prepared carbons (inset: Nyquist plot at high frequency region), (b) Bode diagrams of the real part and (c) the imaginary part of the capacitance vs frequency.

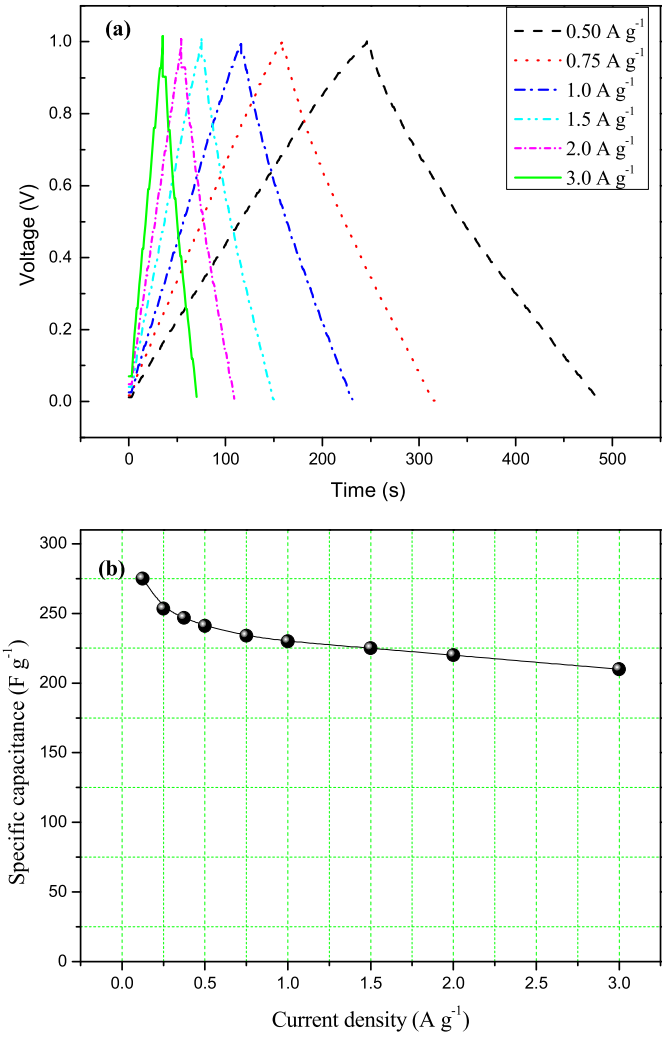


**Fig. 6.** (a) Galvanostatic charge–discharge curves and (b) the specific capacitance of the prepared hierarchical porous carbon at different current densities.

at a high current density of 3 A $g^{-1}$ with a retention of 76%. These electrochemical properties are ascribed to the high surface area and honeycomb-like 3D pore network, providing a favorable pathway for electrolyte transportation. The advantages of this synthesis are: (i) simple self-template approach; (ii) commercially available and cheap raw materials; (iii) excellent electrochemical properties.

## Acknowledgments

This work was financially supported by the National Science Fund for Distinguished Young Scholar (21307075) and the fund from Shanghai Tongji Gao Tingyao Environmental Science & Technology Development Foundation. The authors thank Dr. Pamela Holt for editing the manuscript and 3 anonymous reviewers for helpful suggestions.

## Appendix A. Supplementary data

Supplementary data related to this article can be found, in the online version, at http://dx.doi.org/10.1016/j.jpowsour.2014.07.115.

## References

[1] H. Shen, E. Liu, X. Xiang, Z. Huang, Y. Tian, Y. Wu, Z. Wu, H. Xie, Mater. Res. Bull. 47 (2012) 662–666.
[2] R. Farma, M. Deraman, A. Awitdrus, I.A. Talib, E. Taer, N.H. Basri, J.G. Manjunatha, M.M. Ishak, B.N.M. Dollah, S.A. Hashmi, Bioresour. Technol. 132 (2013) 254–261.

[3] A. Paravannoor, R. Ranjusha, A.M. Asha, R. Vani, S. Kalluri, K.R.V. Subramanian, N. Sivakumar, T.N. Kim, S.V. Nair, A. Balakrishnan, Chem. Eng. J. 220 (2013) 360–366.
[4] X. Li, W. Xing, S. Zhuo, J. Zhou, F. Li, S.-Z. Qiao, G.-Q. Lu, Bioresour. Technol. 102 (2011) 1118–1123.
[5] K. Kim, M. Choi, R. Ryoo, Carbon 60 (2013) 175–185.
[6] E. Raymundo-Piñero, K. Kierzek, J. Machnikowski, F. Béguin, Carbon 44 (2006) 2498–2507.
[7] J. Zhang, L. Jin, J. Cheng, H. Hu, Carbon 55 (2013) 221–232.
[8] K. Xia, Q. Gao, J. Jiang, J. Hu, Carbon 46 (2008) 1718–1726.
[9] X. Zhuang, K. Jia, B. Cheng, X. Feng, S. Shi, B. Zhang, Chem. Eng. J. 237 (2014) 308–311.
[10] S.-h. Du, L.-q. Wang, X.-t. Fu, M.-m. Chen, C.-y. Wang, Bioresour. Technol. 139 (2013) 406–409.
[11] Y. Lv, L. Gan, M. Liu, W. Xiong, Z. Xu, D. Zhu, D.S. Wright, J. Power Sources 209 (2012) 152–157.
[12] W. Huang, H. Zhang, Y. Huang, W. Wang, S. Wei, Carbon 49 (2011) 838–843.
[13] A.M. Baena-Moncada, G.A. Planes, M.S. Moreno, C.A. Barbero, J. Power Sources 221 (2013) 42–48.
[14] Q. Wang, J. Yan, Y. Wang, T. Wei, M. Zhang, X. Jing, Z. Fan, Carbon 67 (2014) 119–127.
[15] H. Xu, Q. Gao, H. Guo, H. Wang, Microporous Mesoporous Mater. 133 (2010) 106–114.
[16] W. Zeng, G. Fang, X. Wang, Q. Zheng, B. Li, H. Huang, H. Tao, N. Liu, W. Xie, X. Zhao, D. Zou, J. Power Sources 229 (2013) 102–111.
[17] J. Yi, X.P. Li, S.J. Hu, W.S. Li, L. Zhou, M.Q. Xu, J.F. Lei, L.S. Hao, J. Power Sources 196 (2011) 6670–6675.
[18] J. Górka, M. Jaroniec, Carbon 49 (2011) 154–160.
[19] M. Pérez-Cabero, F.A. Esteve-Turrillas, D. Beltrán, P. Amorós, Solid State Sci. 12 (2010) 15–25.
[20] A. Özer, G. Gürbüz, A. Çalimli, B.K. Körbahti, Chem. Eng. J. 146 (2009) 377–387.
[21] Y. Li, Q. Du, X. Wang, P. Zhang, D. Wang, Z. Wang, Y. Xia, J. Hazard. Mater. 183 (2010) 583–589.
[22] S. Zhao, B. Gao, Y. Wang, Z. Yang, Colloids Surf. A 417 (2013) 161–169.
[23] Y. Gao, Q. Yue, B. Gao, Y. Sun, W. Wang, Q. Li, Y. Wang, Chem. Eng. J. 232 (2013) 582–590.
[24] I. Stepniak, A. Ciszewski, J. Power Sources 195 (2010) 5130–5137.
[25] T. Thomberg, A. Jänes, E. Lust, Electrochim. Acta 55 (2010) 3138–3143.
[26] P.L. Taberna, P. Simon, J.F. Fauvarque, J. Electrochem. Soc. 150 (2003) A292.
[27] L. Wang, Y. Guo, B. Zou, C. Rong, X. Ma, Y. Qu, Y. Li, Z. Wang, Bioresour. Technol. 102 (2011) 1947–1950.
[28] D. Angın, E. Altintig, T.E. Köse, Bioresour. Technol. 148 (2013) 542–549.
[29] Y. Sun, P.A. Webley, Chem. Eng. J. 162 (2010) 883–892.
[30] U.B. Nasini, V.G. Bairi, S.K. Ramasahayam, S.E. Bourdo, T. Viswanathan, A.U. Shaikh, J. Power Sources 250 (2014) 257–265.
[31] K.Y. Foo, B.H. Hameed, Chem. Eng. J. 173 (2011) 385–390.
[32] Z. Zhang, K. Wang, J.D. Atkinson, X. Yan, X. Li, M.J. Rood, Z. Yan, J. Hazard. Mater. 229-230 (2012) 183–191.
[33] C. Portet, G. Yushin, Y. Gogotsi, Carbon 45 (2007) 2511–2518.
[34] X. Du, W. Zhao, Y. Wang, C. Wang, M. Chen, T. Qi, C. Hua, M. Ma, Bioresour. Technol. 149 (2013) 31–37.
[35] C. Lei, P. Wilson, C. Lekakou, J. Power Sources 196 (2011) 7823–7827.
[36] J. Segalini, B. Daffos, P.L. Taberna, Y. Gogotsi, P. Simon, Electrochim. Acta 55 (2010) 7489–7494.